



Investigating Ca²⁺ salt-based polymer-in-salt electrolyte for future energy storage systems

Kanak Aggarwal¹ · Dipti Yadav¹ · Kashish Tiwari² · Pushpa Kushwaha² · Neelam Srivastava¹

Received: 3 June 2024 / Revised: 16 July 2024 / Accepted: 31 July 2024

© The Author(s), under exclusive licence to Springer-Verlag GmbH Germany, part of Springer Nature 2024

Abstract

The scientific community is continuously putting efforts to improve the energy/power density of energy storage devices, which leads to development of novel materials with enhanced electrochemical properties. Polymer-in-salt electrolytes (PISEs) are expected to have faster ion transport and hence may result in improved power density. In the present study, Ca salt-based PISE is synthesized using glutaraldehyde (GA)-crosslinked arrowroot starch as host matrix. The synthesized PISE has high conductivity (~0.01 S/cm), wide electrochemical stability window (ESW > 3 V), and small characteristic relaxation time ($\tau \sim 17 \mu\text{s}$) indicating the possibility of faster response in any device fabricated using synthesized PISEs. Fabricated supercapacitor, using the highest conducting PISE with rGO as electrode, has specific capacitance ~ 17 F/g at 1 mV/s and high power density 2.1 kW/kg with coulombic efficiency (CE) of > 90.05% and with CAC as electrode, specific capacitance ~ 125 F/g at 1 mV/s and high power density 2.1 kW/kg with coulombic efficiency (CE) of > 99%.

Keywords RGO · Polymer-in-salt electrolytes · Supercapacitor · Calcium · Activated carbon · Arrowroot starch

Introduction

The hunt for improved electrode and electrolyte materials, so that performance of energy devices can be enhanced, is an ever-lasting process. The progress in the field of electrode materials is quite appreciating [1–4], but to demonstrate the performance of any new electrode materials, the scientific community still uses liquid electrolytes [5–8]. The bigger size of the ions requiring larger space for movement leads to poor conductivity in solid physique [9, 10]. But with liquid electrolytes, the problems of lower electrochemical stability window, corrosion, and packaging-related issues have been faced. Few organic electrolytes and ionic liquid-based electrolytes have shown better performance but they are not cost-effective. Polymer electrolytes are widely being used

at commercial level but additives are required to achieve the desired electrochemical properties [11–14]. After the work of Angell and co-authors in 1990s [15–17], polymer-in-salt electrolytes (PISEs) came as a possible alternate to have faster ion movement in solid-state electrolytes, but the efforts in the field still did not reach commercial applications. In PISEs, ion transport is not only faster but it may also have greater cationic transference number, a well-desired property of the electrolytes [18, 19]. PISEs offer a possibility to blend the fast-ionic conduction of glassy electrolytes with the required mechanical properties of rubbery polymers [20]. In the case of PISEs, the ion motion is decoupled from polymer segmental motion, and due to its diffusion through ion clusters, it is much faster. Even after so many promising characteristics, the PISEs are not reaching commercial level because of brittleness of lattice at higher salt concentration, recrystallization of salt, need of eutectic salt combination which can remain in molten state at room temperature so that by adding a small amount of polymer a better electrolyte can be achieved. Previous studies indicate [21, 22] that a loosely bonded host matrix may lead to better PISE. In few recent studies, it has also been pointed out that polymer hosts which can be broken into small molecules by addition of salts may also lead to better PISEs [23–25]. With Na and Mg salts, it has been proved that crosslinked starches

Kanak Aggarwal and Dipti Yadav contributed equally to the present work.

✉ Neelam Srivastava
neel@bhu.ac.in

¹ Department of Physics (MMV), Banaras Hindu University, Varanasi, India

² Department of Physics, Jawaharlal Nehru University, New Delhi, India

are quite good host for ecofriendly, economical, and flexible PISEs which are free from aging effects/recrystallization problems, and hence in the present study, Ca salt-based PISE is being synthesized and characterized for their energy device fabrication. Calcium is the 5th most abundant element on the earth's crust that can make energy devices more cost-effective [26], and studies on the development of Ca-based energy devices are in an early stage [27] relative to the well-studied electrolyte systems based on Li^+ [28, 29], Na^+ [30, 31], K^+ [32], Mg^{2+} [33, 34], and Al^{3+} [35, 36]. In the present work, glutaraldehyde (GA)-crosslinked starch has been used as host matrix. Crosslinking it with glutaraldehyde not only makes the system fungal-free but it also leads to flexible films which can be molded into different sizes and shapes. Although crosslinking with GA leads to many favorable properties, there is an optimum value after which other problems are seen in the material [37, 38]. To the best of the author's knowledge, understanding of the Ca-based PISEs is not reported till date and hence this work is an attempt to understand that the same Ca is the fifth most abundant element naturally found in earth's crust which is attracting scientific community for its application in energy devices [39, 40]. CaCl_2 is used as this can be dissolved in solvents like methanol due to its low dissociation energy [41] which makes electrolyte synthesis non-toxic in nature. The primary goal of our study is to develop environmentally benign and cost-effective systems, which is why it was chosen to employ CaCl_2 as the material for energy device applications [42].

To develop an understanding of the electrochemical properties of calcium-based polymer electrolytes, a series of electrolytes have been synthesized from 25 wt% salt to 72 wt% salt with crosslinked starch as a host polymer. Since the aqueous electrolytes are the most promising electrolytes (if the smaller ESW and designing problems are neglected),

efforts are being made to have water-based electrolytes in solid state [43, 44] and a new nomenclature "Water-in-Polymer Salt electrolytes (WiPSEs)" [45, 46] has recently appeared in literature. In the present study, efforts have also been made to enhance the moisture content of the synthesized PISE by exposing it in a high humidity atmosphere.

Experimental details

Materials

Arrowroot starch, calcium chloride dihydrate (Sigma-Aldrich, 99% purity), glutaraldehyde (Merck, Product Code 8.20603.0521), methanol (Qualigens, HPLC grade (assay percentage range 99.8%)), carbon black (Super P, 99% purity) (Alfa Aesar), polyvinyl alcohol (PVA) (Sigma-Aldrich, Product Code 363,081), distilled water (lab prepared).

Electrolyte preparation

Arrowroot starch, calcium chloride, glutaraldehyde, and methanol were used to prepare the sample. Solid polymer electrolyte films were prepared at room temperature (40 °C) using the solution cast technique as used previously in our lab for synthesis [47–49] as shown in Fig. 1a. A series of electrolytes were prepared using 0.5 g of starch with different amounts of salt 0.25 g, 0.5 g, 0.75 g, 1.0 g, and 1.25 g, and for further discussion, they are named 25wt%, 50wt%, 60wt%, 66wt%, and 72wt%. For the preparation of 25 wt% electrolyte, 0.5 g of starch was added to 10 ml methanol and left to continuously stir for 1 h at room temperature (40 °C). In a separate beaker, 0.25 g of salt was added to 10 ml methanol, and the mixture was continuously stirred for 1 h

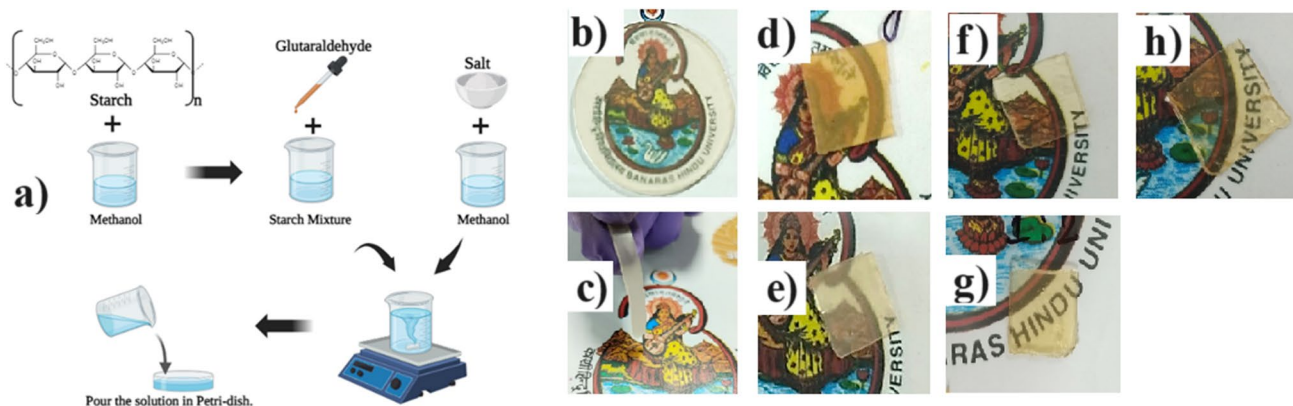


Fig. 1 a Protocol for synthesis of polymer electrolyte film. b Image of synthesized PISE film at 72wt%. c Image showing ease of handling of PISE at 72wt%. Image of electrolyte at d 25wt%, e 50wt%, f 60wt%, g 66wt%, and h 72wt%

at room temperature. Then, 1 ml glutaraldehyde is added to the starch mixture and left for continuous stirring for 30 min. Then, salt mixture was added to the starch mixture and stirred at a constant speed (350 rpm) and the whole mixture was left to stir till a homogenous mixture was obtained. After this, a homogeneous mixture was poured into the petri dish and was left to dry at ambient for almost 10 days to obtain a transparent, free-standing film as shown in Fig. 1. Same protocol is followed for all salt concentrations.

Preparation of electrodes

Commercial rGO and commercial activated carbon (CAC) were used as two types of electrode material for the comparative study of the charge storage mechanism by fabricating a supercapacitor. The slurry was prepared using distilled water and 80wt% of active material (CAC, rGO), 10wt% conducting agent (Super P), and 10wt% of binder (PVA, Sigma-Aldrich). Firstly, add PVA into distilled water and left for stirring till it dissolves. After dissolving PVA in distilled water, add Super P, active material (CAC or rGO), and stir for 3 h to get slurry. The prepared slurry was coated on carbon cloth using the doctor blade technique and was left to dry at 100 °C for 3 h. The weight of the loaded active material is 0.24 mg/cm² for rGO and 0.24 mg/cm² for CAC. The obtained electrodes were used for the characterization.

Structural and electrochemical characterization

XRD measurements were recorded over the range of diffraction angle 5° to 80° done using D2 Phaser Bruker. For moisture content analysis of electrolytes, the HS153 moisture analyzer machine of Metler Toledo was used. The electrochemical impedance spectroscopy (EIS), linear sweep voltammetry (LSV), cyclic voltammetry (CV), and galvanostatic charging discharging (GCD) were carried out using a two-electrode setup using CHI660E. The conductivity of the electrolyte was calculated using the following equation [50]:

$$\sigma = l/(R \times A) \quad (1)$$

Here, R denotes the ESR (ohm) value of the electrolyte, and l and A represent the thickness of the electrolyte and surface area of contact of electrode/electrolyte in cm² respectively. σ represents the conductivity. The specific capacitance using GCD plot of the fabricated supercapacitor was calculated using the formula:

$$C = \frac{(I \cdot \Delta t)}{(m \cdot \Delta V)} \quad (2)$$

Here, C represents the specific capacitance of the fabricated supercapacitor in units of F/g. (I/m) is the current density. Δt is discharging time from GCD plot, m is the mass of the active material, and ΔV is the voltage range.

The specific capacitance using the cyclic voltammetry curve of the fabricated supercapacitor was calculated using the formula:

$$C = (\int IdV)/(2mVs) \quad (3)$$

Here, C represents the specific capacitance of the fabricated supercapacitor in units of F/g. $\int IdV$ is the area enclosed in CV curve. s is the scan rate (V/s), m is the mass of the active material, and V is the voltage range.

The values of specific energy density (E) and power density (P) were calculated using the following formula [51, 52]:

$$E(\text{W h/kg}) = ((0.5) \times (CV^2))/3.6 \quad (4)$$

$$P(\text{W/kg}) = (E/t)3600 \quad (5)$$

$$\eta = t_d/t_c \times 100\% \quad (6)$$

Here, C is specific capacitance (F/g), V is the potential change after IR drop, and t (s) is discharging time in GCD plot. Here, η represents coulombic efficiency (%) where t_d and t_c are the time of discharging and charging of the supercapacitor.

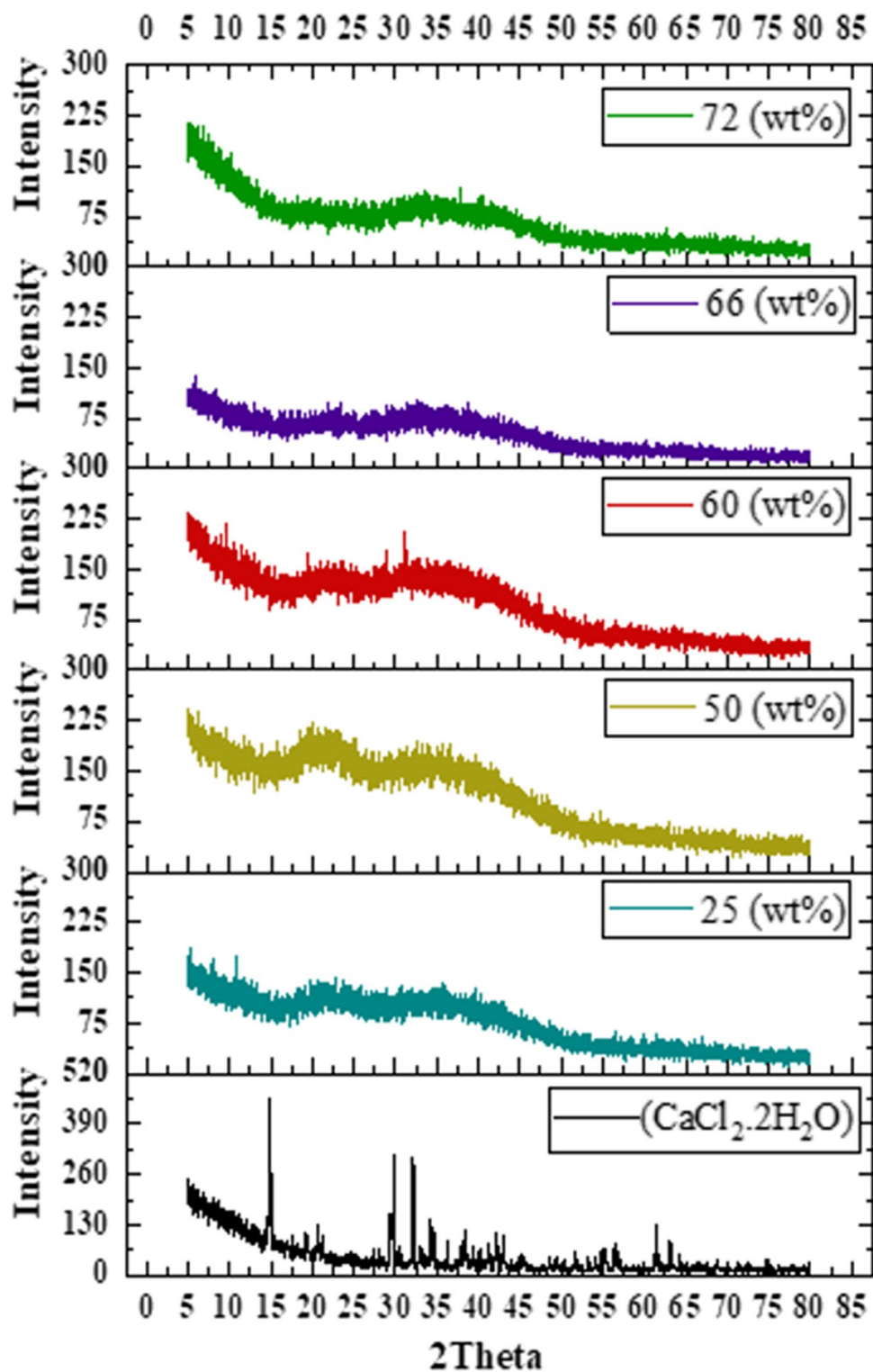
Results

Structural characterization

The biggest hurdle in the path of PISEs reaching commercial level is recrystallization of salt at high salt concentrations. Hence, while characterizing PISEs, XRD comes as the most basic analysis as it provides information on whether the crystallinity is present in the electrolyte or not. Hence, XRD is used to understand the crystalline and amorphous nature of prepared electrolytes [53] from salt-in-polymer electrolyte (SIPE) to PISE range. Figure 2 shows the XRD spectra of pure salt (CaCl₂·2H₂O) and synthesized electrolytes from 25wt% salt to 72wt% salt. In XRD data, distinct XRD peaks could be seen only in pure salt which is found to be identical to the JCPDS data (ICCD-PDF 01-070-0385). It is observed that the crystalline nature of pure salt has completely disappeared at 25wt% salt itself. While shifting salt concentration from 25wt% to 72wt%, no recrystallization is detected in XRD spectra, which means complete acceptance of salt by crosslinked starch matrix without recrystallization.

The present system has an edge over the systems reported [54, 55] with synthetic polymers as host matrix, as the XRD data indicates that the amorphicity is continuously enhancing with salt concentration. The

Fig. 2 XRD spectra of CaCl_2 salt along with 25 wt% (SIPE) to 72 wt% (PISE) of salt used for electrolyte formulation



possible reasons for this may be (i) breaking of starch molecules into smaller molecules by salt [25] which leads to enhanced availability of ion-interacting moieties and also enhances the possibility of hydrogen bonding leading

to loosely bonded structure (ii) enhance moisture content with salt concentration which also support better interaction of ions and starch through hydrogen bonding via these water molecules.

Electrochemical performance of synthesized electrolytes

Electrochemical impedance spectroscopy was used for analyzing the effect of salt concentration on the conductivity of the electrolytes with salt concentration performed in the range of 1 Hz to 1 MHz. Conductivity and ESW have been analyzed to understand the electrochemical behavior of synthesized electrolytes. Impedance data has been analyzed by Nyquist plots and is given in Fig. 3a.

The straight-line nature of Nyquist plot which intercepts at very low resistance indicates high conductivity of the synthesized PISE. Nyquist plots indicate that as the salt concentration is increased the resistance is continuously decreasing. The conductivity vs salt concentration plot given in Fig. 3c indicates a jump at nearly 50wt% salt concentration which may be correlated with transition from SIPE to PISE transport mechanism. LSV curves for all five synthesized

electrolytes are given in Fig. 3b and the ESW estimated from these curves are summarized in Table 1.

ESW is quite wide, ~ 4 V for all electrolytes. A decrease in ESW with salt concentration is an obvious [48–50, 56–58] phenomenon because as the salt concentration increases, there are more number of fast moving ions and hence can be easily oxidized/reduced leading to a lowered value of ESW.

The value of ESW depends on the combination of electrolyte and electrode [59] resulting to the limits of the maximum energy density and power density of the system [60]. Here, it is evaluated by using an Al electrode to study the ESW of the prepared series of SIPE to PISE in order to understand the electrochemical stability of the material. Al/ electrolyte/Al composition is used to estimate the ESW and Fig. 3b shows the LSV curves for electrolytes with different salt concentrations. It is observed that from SIPE to PISE, ESW has decreased.

Fig. 3 **a** Nyquist plot for prepared materials having different salt concentrations (mentioned salt wt% in total material). **b** ESW for all synthesized polymer films with different wt% of salt present in electrolyte films as mentioned in the curve. **c** Variation of conductivity with variation of wt% of salt concentration in polymer films. **d** Ratio of parallel capacitance and series capacitance C_p/C_s graph with log frequency

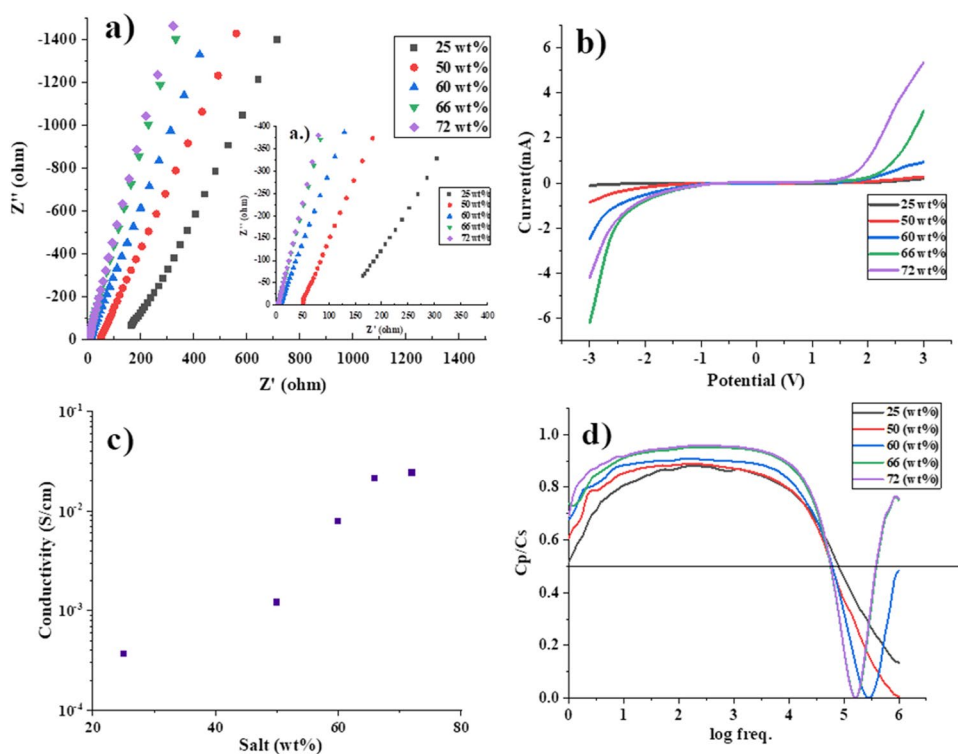


Table 1 Values of ESR, ESW, conductivity, moisture content, and relaxation time with variation in salt concentration

Salt (wt%)	Phase angle (Max)	ESR (Ω)	ESW (V)	Thickness (cm)	Conductivity (S/cm)	Moisture (%)	Relaxation times (μ s)
25	69.80	177	5.2	0.065	3.65×10^{-4}	26.73	12.4
50	70.40	51	4.3	0.063	1.21×10^{-3}	27.07	16.2
60	72.40	9	4.2	0.071	7.88×10^{-3}	31.48	16.2
66	77.30	4	4	0.09	2.11×10^{-2}	31.37	17.1
72	78.20	4.22	3.7	0.102	2.42×10^{-2}	34.17	17.4

The value of relaxation time is estimated from the frequency at which the value of C_p/C_s is 0.5 [61] as shown in Fig. 3d and values for different salt concentrations are summarized in Table 1. Although, for both SIPE and PISE, the relaxation time τ is in μs range, the resistance values of SIPE and PISE are different that can be associated with difference in the available number of charge carriers in two ranges. The estimated relaxation times are in μs range indicating faster ion transport in synthesized electrolytes, which can be associated with high moisture content in the system leading to aqueous type of electrolyte behaviors.

Humidity/moisture content (MC) effect on ESR

Aqueous electrolytes are well established, but due to leakage/designing problems, their solid-state alternates are always sought. In this hunt, for achieving aqueous electrolyte properties in solid state, with wider electrochemical stability window (ESW), a new class of electrolytes classified as “Water-In-Salt-Electrolytes”, or “Water-In-Polymer-Salt-Electrolytes” [43–46], are being explored by the researchers. Here, in the present system where the salt and starch both have an affinity for water, a novel approach has been adopted to stabilize water in the polymer matrix. Moisture content seems to play a favorable role in stopping the recrystallization by keeping the matrix flexible and easy to handle for design purposes.

Hence, to develop the understanding of synthesized electrolytes, MC and resistance of the synthesized samples have been measured at different relative humidities in series of

five steps, as mentioned in Table 2. A difference between the behavior of SIPE and PISEs at different humidity levels is observed. In the case of SIPE, resistance drastically changes varying from $\sim 3\Omega$ (at 99% RH) to 9358Ω (at 22%) whereas in the case of PISEs the variation is very small. It indicates that in the case of SIPE either the H^+ or OH^- from absorbed water are moving or water is assisting the movement of cation/anion from salt.

ESW of these three samples were also measured at different humidity levels. The results are very interesting and in accordance to the previous patent from our group. In SIPE region at 99% RH, the ESW is almost zero indicating that the absorbed water molecules are easily dissociated [62], whereas on moving towards higher salt concentration water molecules are stabilized [46, 63–65]. At normal ambient humidity ($\sim 60\%$ RH), the ESW is $> 2.5\text{ V}$ which is quite wide for device fabrication. The effect of different humidity exposures on the moisture content and Nyquist are shown in Fig. 2S-12S.

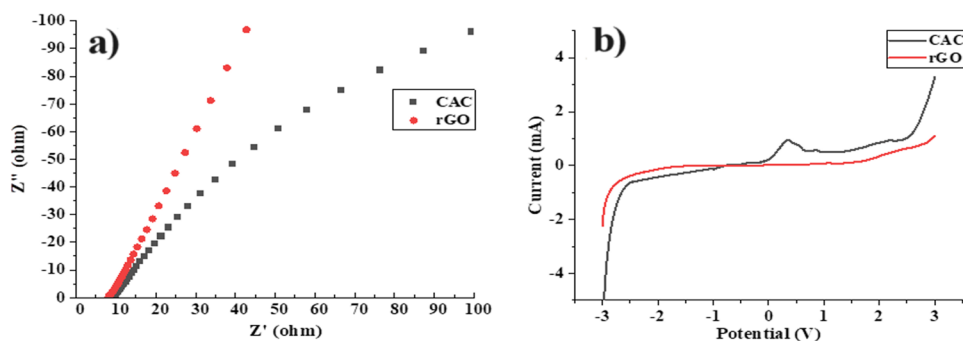
Supercapacitor performance using activated carbon and rGO

To understand the possible application of synthesized electrolytes for energy device fabrication, two symmetric supercapacitors are fabricated, with commercially available active electrode materials namely (i) rGO and (ii) activated carbon (CAC). Active materials are coated on carbon cloths to be used as electrode. In both the cases, the configuration used is electrode/electrolyte/separator/electrolyte/electrode with

Table 2 Effect of different relative humidities on the ESR (ohm), ESW (V), and moisture content (%) of the 25 wt%, 60 wt%, and 72 wt%

	Humidity	25 (wt%) salt			60 (wt%) salt			72 (wt%) salt		
		ESR (Ω)	MC%	ESW (V)	ESR (Ω)	MC%	ESW (V)	ESR (Ω)	MC%	ESW (V)
Step 1	60%	54.34	21.21	5.3	3.02	24.11	4.2	2.05	34.65	3.69
Step 2	22%	9358	9.35	6	37.03	16.67	5.24	12.79	17.21	3.75
Step 3	99%	2.77	33.67	0	1.56	52.94	1.1	1.44	47.60	1.4
Step 4	22%	9172	7.62	6	15.61	6.93	2.6	10.47	19.29	2.8
Step 5	88%	14.25	34.58	4.4	1.38	44.21	2.38	1.8	45.31	2.1

Fig. 4 **a** Nyquist of prepared supercapacitor devices using CAC and rGO electrode material. **b** Linear sweep voltammetry graphs of fabricated supercapacitors using CAC and rGO as electrode material



commercial tissue paper (cellulose based) as a separator. The values of ESR estimated from Nyquist plots given in Fig. 4a are 9.25 Ω for CAC electrode and 8 Ω for rGO electrode. The electrochemical stability window (ESW) were estimated from LSV curve given in Fig. 4b. The ESW value obtained for rGO electrode is > 2.5 V but obtained ESW > 2 V for CAC electrode. The difference between the ESW for two systems can be correlated with the size of ion clusters with surface area as well as the pore size of electrode material [66].

CV curve of devices with rGO and CAC electrode are shown in Fig. 5 a and b at different scan rates ranging from 1 to 10 mV/s. The values of specific capacitance calculated using CV plots are found to be 17 F/g and 125 F/g respectively for rGO and CAC electrode materials

using Eq. (3) at 1 mV/s scan rate as mentioned in Table 3. CV curves with rGO are more rectangular in comparison to CAC-based systems indicating EDLC type nature of rGO-based supercapacitor. Specific capacitance estimated as a function of scan rate is given in Fig. 5c, which shows quite a stable behavior, while CAC electrode based supercapacitor shows pseudocapacitive behavior which can state that the charge transfer between the electrode and electrolyte occurs as a result of a faradic current passing through the supercapacitor in pseudocapacitors, which store energy by faradaic reaction, intercalation, or electrosorption [5] that may have resulted in the higher specific capacitance in CAC-based supercapacitors. The variation of specific capacitance with scan rate for CAC electrode is shown in Fig. 5d.

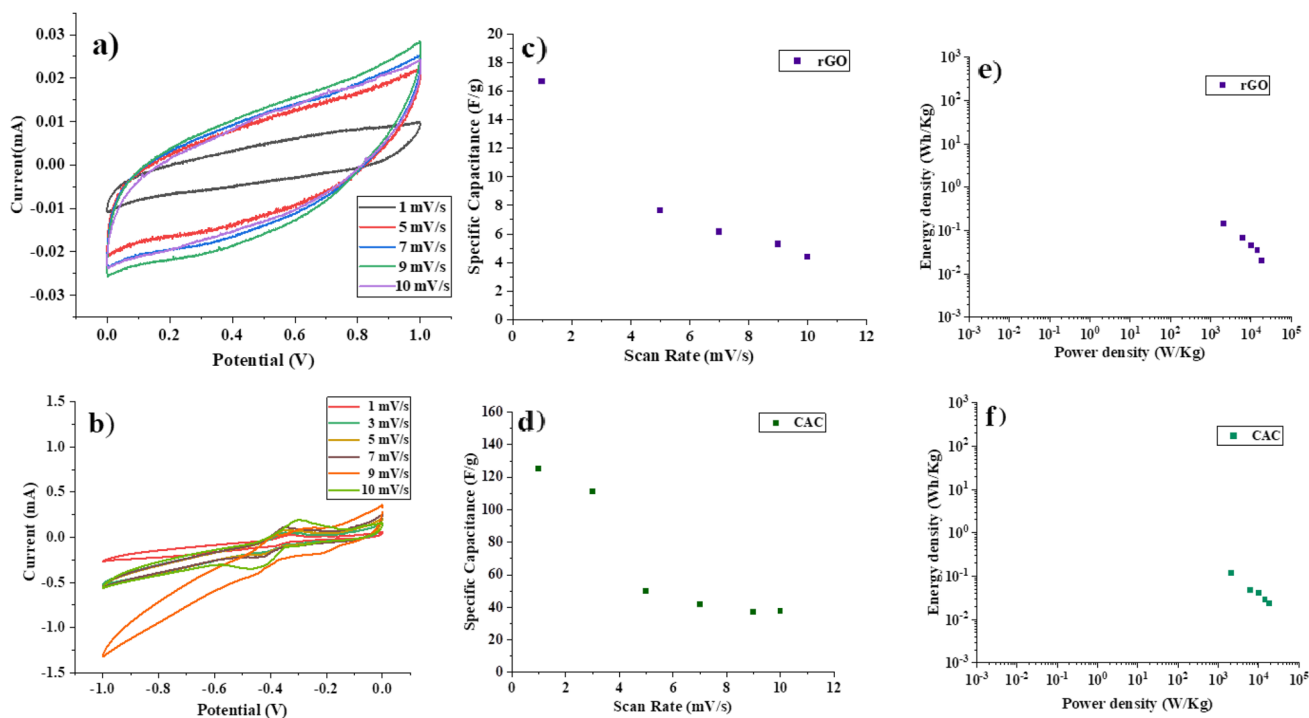


Fig. 5 Cyclic voltammograms (CV) of fabricated supercapacitor scan rate ranging from 1 to 10 mV/s using **a** rGO electrode and **b** CAC electrode. Value of variation in specific capacitance with variation

in the scan rate using **c** rGO electrode and **d** CAC electrode. Ragone plot for comparing the category of energy device fabricated using **e** rGO electrode and **f** CAC electrode

Table 3 Variation in specific capacitance, energy density of rGO- and CAC-based supercapacitors, calculated by using CV plots

Sr. No	Scan rate (mV/s) (CAC)	Specific capacitance (F/g) (CAC)	Energy density (Wh/kg) (CAC)	Scan rate (mV/s) (rGO)	Specific capacitance (F/g) (rGO)	Energy density (Wh/kg) (rGO)
1	1	125	17.40	1	17	2.32
2	5	50	6.94	5	8	1.06
3	7	41	5.79	7	6	0.86
4	9	37	5.14	9	5	0.73
5	10	37	5.21	10	4	0.61

There is a small variation in the value of specific capacitance with scan rate because at low scan rates (1 mV/s) the larger electrode surface is utilized for electrochemical reaction and at higher scan rates a limited surface area of electrodes can be utilized resulting in low value of capacitance [67]. At high scan rates, the high diffusion resistance which could be because of meager ion migration and ion diffusion affecting the ions' movements between electrode and electrolyte results in decreased specific capacitance [68].

The two most popular electrochemical energy storage technologies among the different energy storage devices are batteries and supercapacitors, as seen in a graph known as a Ragone plot that shows energy density in Wh/kg vs. power density in W/kg as shown in Fig. 5 e and f. Using the Ragone plot, it can be found that in the studied energy storage systems power density lies in the range of 10^3 – 10^4

W/kg and energy density in the range of (10^{-1} – 10^{-2}) Wh/kg, which belongs to the category of supercapacitors or ultracapacitors [69, 70].

Analysis of charging-discharge curve

Galvanostatic charging-discharging (GCD) has been carried out to access the charge and discharge characteristic of rGO- and CAC-based supercapacitors, ranging from current density 4 A/g to 37.5 A/g. Figure 6 a and b show the charging-discharging plot for rGO- and CAC-based supercapacitor. It is observed that time taken for the charging-discharging of cycles is ~ 0.5 s that may be due to the low relaxation time and high conductivity of electrolyte material. Charging-discharging test of rGO and CAC electrode is carried out till 5000 cycles to check the stability of the system

Fig. 6 Charging-discharging plot of fabricated supercapacitor using **a** rGO electrode and **b** CAC electrode. Coulombic efficiency up to 5000 cycles using **c** rGO electrode and **d** CAC electrode

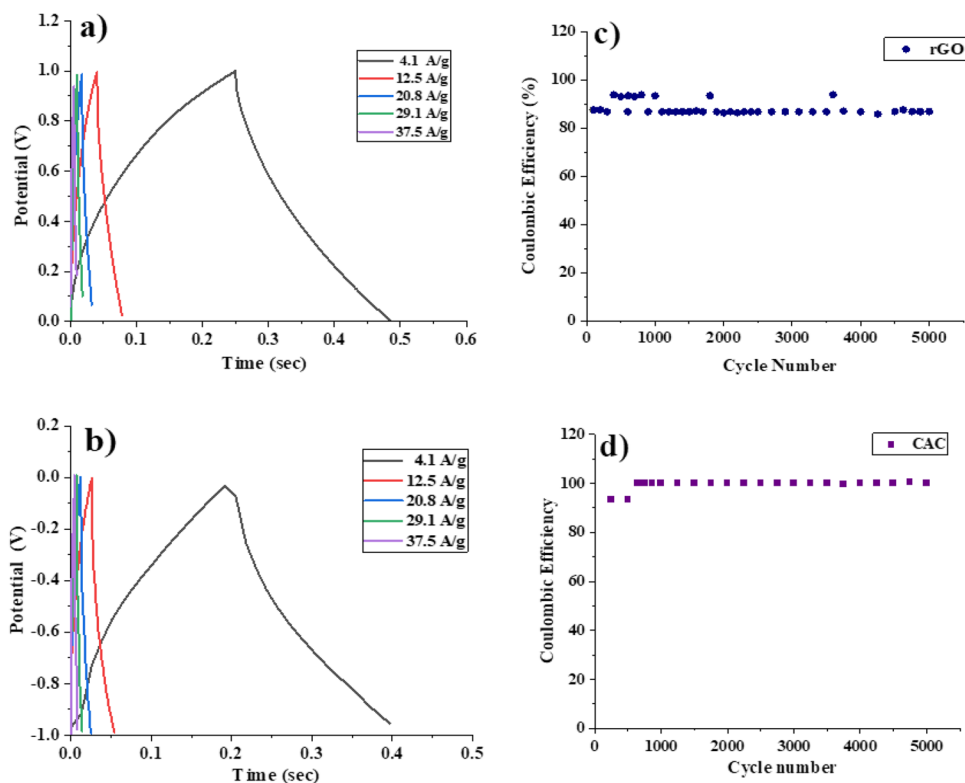


Table 4 Variation in specific capacitance, energy density, and power density of rGO- and CAC-based supercapacitors, calculated by using GCD plots

Sr No	Current density (A/g)	Specific capacitance (F/g)		Energy density (Wh/kg)		Power density (kW/kg)	
		CAC	rGO	CAC	rGO	CAC	rGO
1	4.17	0.86	1.02	0.12	0.14	2.1	2.1
2	12.50	0.35	0.48	0.05	0.07	6.3	6.3
3	20.83	0.29	0.32	0.04	0.04	10.4	10.4
4	29.17	0.21	0.25	0.03	0.03	14.6	14.6
5	37.50	0.17	0.14	0.02	0.02	18.8	18.8

as a supercapacitor at 4 A/g. Charging-discharging curve shows triangular shape cycles [71, 72] which indicates the fast ion transport in fabricated supercapacitor at different current densities in the 0–1 V voltage range.

The values of energy and power density are mentioned in Table 4 and are found to be 0.14 Wh/kg, 2.1 kW/kg, and 0.12 Wh/kg, 2.1 kW/kg that are comparable to the other reported systems [73–75] which is due to the short relaxation time of the synthesized electrolytes. Figure 6 c and d show the value of coulombic efficiency found to be (η %) > 90% for rGO-based supercapacitors and the value of coulombic efficiency is found to be (η %) > 99% in CAC-based supercapacitor.

Conclusions

GA-crosslinked arrowroot starch doped with CaCl_2 salt-based polymer electrolytes is studied for the SIPE to PISE range, by using a simple synthesis protocol which satisfies the three “E” conditions (environment friendly, easy to prepare, economical) required for commercial application. Here, success has been achieved to keep it free from recrystallization problem without the need of any additives and/or the requirement of molten salt/salts which makes it an interesting material. High humidity exposure of PISE films resulted in ambient stabilized electrolyte with high conductivity, which could be considered aqueous electrolyte in solid-state physique. Small relaxation time ($\sim 17 \mu\text{s}$) and high conductivity (10^{-2} S/cm) with high ESW range ($> 3.5 \text{ V}$) make the synthesized polymer electrolyte film a potential candidate for future commercial testing. Supercapacitors are fabricated using commercially available activated carbon (CAC) and reduced graphene oxide (rGO). rGO-based supercapacitor is having EDLC behavior whereas CAC-based supercapacitor has pseudocapacitance type of nature. Faster charging-discharging cycles are obtained because of PISE films, which results in high power density values. Although the energy and power density estimated from GCD techniques results in almost similar energy and power density behavior for both the systems, CAC-based supercapacitor seems to have better coulombic efficiency ($\sim 99\%$) in comparison to rGO-based supercapacitor ($\sim 90\%$), which indicates long life and stable behavior. Achieved power density is of the order of kW/kg which adds up to favorable properties for commercial application.

Supplementary Information The online version contains supplementary material available at <https://doi.org/10.1007/s11581-024-05754-4>.

Acknowledgements Author NS is thankful to BHU for providing research grant for faculty (IOE Scheme) DeV scheme No 6031- sanction number R/DeV/D/IOE/Incentive/2021-22/32161 and also infra structure grant sanction number R/Dev/D/Object head

35/2018-19/73496. Authors acknowledge the CIL (central instrumentation lab) MMV, BHU for providing facility for XRD measurement. Author KA, DY is thankful to Banaras Hindu University for providing UGC research fellowship.

Author contribution NS is Ph.D. supervisor of KA and DY and has framed the scientific work and finalized the manuscript. KA and DY have equal contribution in doing the experimental work and conceptualizing of scientific content. Kashish Tiwari and Pushpa Kushwaha did some experimental and calculation work as a summer intern.

Funding Author NS is thankful to BHU for providing research grant for faculty (IOE Scheme) DeV scheme No 6031- sanction number R/DeV/D/IOE/Incentive/2021-22/32161 and also infrastructure grant sanction number R/Dev/D/Object head 35/2018-19/73496. Authors KA and DY are thankful to Banaras Hindu University for providing UGC research fellowship. NS is thankful to SRICC credit research incentive for faculty members (SRICC/IOE/CRI(FM)/2022-23/2724).

Data availability No datasets were generated or analysed during the current study.

Declarations

Competing interests The authors declare no competing interests.

References

- Kim H, Kim H, Ding Z, Lee MH, Lim K, Yoon G, Kang K (2016) Recent progress in electrode materials for sodium-ion batteries. *Adv Energy Mater* 6:1600943. <https://doi.org/10.1002/aenm.201600943>
- Jin H, Li J, Yuan Y, Wang J, Lu J, Wang S (2018) Recent progress in biomass-derived electrode materials for high volumetric performance supercapacitors. *Adv Energy Mater* 8. <https://doi.org/10.1002/aenm.201801007>
- Xu Y, Yu S, Johnson HM, Wu Y, Liu X, Fang B, Zhang Y (2024) Recent progress in electrode materials for micro-supercapacitors. *iScience* 27. <https://doi.org/10.1016/j.isci.2024.108786>
- Sharma SK, Sharma G, Gaur A, Arya A, Mirsafi FS, Abolhassani R, Rubahn HG, Yu JS, Mishra YK (2022) Progress in electrode and electrolyte materials: path to all-solid-state Li-ion batteries. *Energy Adv* 1:457–510. <https://doi.org/10.1039/d2ya00043a>
- Anandhi P, Harikrishnan S, Senthil Kumar VJ, Lai WC, Mahmoud AED (2022) The enhanced energy density of rGO/TiO₂ based nanocomposite as electrode material for supercapacitor. *Electronics (Switzerland)* 11:1792. <https://doi.org/10.3390/electronics11111792>
- Sankar KV, Selvan RK (2015) Improved electrochemical performances of reduced graphene oxide based supercapacitor using redox additive electrolyte. *Carbon N Y* 90:260–273. <https://doi.org/10.1016/j.carbon.2015.04.023>
- Rajasekaran SJ, Grace AN, Jacob G, Alodhayb A, Pandiraj S, Raghavan V (2023) Investigation of different aqueous electrolytes for biomass-derived activated carbon-based supercapacitors. *Catalysts* 13:286. <https://doi.org/10.3390/catal13020286>
- Snook GA, Kao P, Best AS (2011) Conducting-polymer-based supercapacitor devices and electrodes. *J Power Sources* 196:1–12
- Li H, Han C, Huang Y, Huang Y, Zhu M, Pei Z, Xue Q, Wang Z, Liu Z, Tang Z, Wang Y (2018) An extremely safe and wearable solid-state zinc ion battery based on a hierarchical structured polymer electrolyte. *Energy Environ Sci* 11:941–951. <https://doi.org/10.1039/c7ee03232c>

10. Wang J, Lei G, He T, Cao H, Chen P (2022) Defect-rich potassium amide: a new solid-state potassium ion electrolyte. *J Energy Chem* 69:555–560. <https://doi.org/10.1016/j.jechem.2022.01.046>
11. Liu W, Yi C, Li L, Liu S, Gui Q, Ba D, Li Y, Peng D, Liu J (2021) Designing polymer-in-salt electrolyte and fully infiltrated 3D electrode for integrated solid-state lithium batteries. *Angewandte Chemie* 133:13041–13050. <https://doi.org/10.1002/anie.202101537>
12. Wu H, Gao P, Jia H, Zou L, Zhang L, Cao X, Engelhard MH, Bowden ME, Ding MS, Hu J, Hu D (2021) A polymer-in-salt electrolyte with enhanced oxidative stability for lithium metal polymer batteries. *ACS Appl Mater Interfaces* 13:31583–31593. <https://doi.org/10.1021/acscami.1c04637>
13. Ma Q, Liu D, Wang B, Liu W, Xiong G, Liu J (2023) Cellulose acetate-promoted polymer-in-salt electrolytes for solid-state lithium batteries. *J Solid State Electrochem* 27:1411–1421. <https://doi.org/10.1007/s10008-023-05414-z>
14. Chattopadhyay J, Pathak TS, Santos DMF (2023) Applications of polymer electrolytes in lithium-ion batteries: a review. *Polymers* 15:3907
15. Angell CA (2017) Polymer electrolytes—some principles, cautions, and new practices. *Electrochim Acta* 250:368–375. <https://doi.org/10.1016/j.electacta.2017.07.118>
16. Angell CA (1992) Mobile ions in amorphous solids. *Annu Rev Phys Chem* 43:693–717. <https://doi.org/10.1146/annurev.pc.43.100192.003401>
17. Angell CA, Liu C, Sanchez E (1993) Rubbery solid electrolytes with dominant cationic transport and high ambient conductivity. *Nature* 362:137–139. <https://doi.org/10.1038/362137a0>
18. Kumar M, Tiwari T, Srivastava N (2012) Electrical transport behaviour of bio-polymer electrolyte system: potato starch + ammonium iodide. *Carbohydr Polym* 88:54–60. <https://doi.org/10.1016/j.carbpol.2011.11.059>
19. Wischniewski A, Monkenbusch M, Willner L, Richter D, Kali G (2003) Direct observation of the transition from free to constrained single-segment motion in entangled polymer melts. *Phys Rev Lett* 90:058302. <https://doi.org/10.1103/PhysRevLett.90.058302>
20. Gao H, Grundish NS, Zhao Y, Zhou A, Goodenough JB (2021) Formation of stable interphase of polymer-in-salt electrolyte in all-solid-state lithium batteries. *Energy Material Advances*. <https://doi.org/10.34133/2021/1932952>
21. Wright PV (1976) An anomalous transition to a lower activation energy for dc electrical conduction above the glass-transition temperature. *J Polym Sci Polym Phys Ed* 14:955–957. <https://doi.org/10.1002/pol.1976.180140516>
22. Wright PV (1998) Polymer electrolytes - the early days. *Electrochim Acta* 43:1137–1143. [https://doi.org/10.1016/S0013-4686\(97\)10011-1](https://doi.org/10.1016/S0013-4686(97)10011-1)
23. Wang Z, Gao W, Chen L, Mo Y, Huang X (2002) Study on roles of polyacrylonitrile in “salt-in-polymer” and “polymer-in-salt” electrolytes. *Solid State Ion* 154:51–56. [https://doi.org/10.1016/S0167-2738\(02\)00463-0](https://doi.org/10.1016/S0167-2738(02)00463-0)
24. Moreau L, Bindzus W, Hill S (2011) Influence of salts on starch degradation: Part I - sodium chloride. *Starch/Staerke* 63:669–675. <https://doi.org/10.1002/star.201100031>
25. Moreau L, Bindzus W, Hill S (2011) Influence of salts on starch degradation: Part II - salt classification and caramelisation. *Starch/Staerke* 63:676–682. <https://doi.org/10.1002/star.201100032>
26. Monti D, Ponrouch A, Araujo RB, Barde F, Johansson P, Palacín MR (2019) Multivalent batteries-prospects for high energy density: Ca batteries. *Front Chem* 7:79. <https://doi.org/10.3389/fchem.2019.00079>
27. Arroyo-De Dompablo ME, Ponrouch A, Johansson P, Palacín MR (2019) Achievements, challenges, and prospects of calcium batteries. *Chem Rev* 120:6331–6357
28. Sun M, Zeng Z, Zhong W, Han Z, Peng L, Yu C, Cheng S, Xie J (2022) In situ prepared “polymer-in-salt” electrolytes enabling high-voltage lithium metal batteries. *J Mater Chem A Mater* 10:11732–11741. <https://doi.org/10.1039/d2ta00093h>
29. Ma L, Kim MS, Archer LA (2017) Stable artificial solid electrolyte interphases for lithium batteries. *Chem Mater* 29:4181–4189. <https://doi.org/10.1021/acs.chemmater.6b03687>
30. Delmas C (2018) Sodium and sodium-ion batteries: 50 years of research. *Adv Energy Mater* 8:1703137
31. Lu Y, Li L, Zhang Q, Niu Z, Chen J (2018) Electrolyte and interface engineering for solid-state sodium batteries. *Joule* 2:1747–1770
32. Gao H, Xue L, Xin S, Goodenough JB (2018) A high-energy-density potassium battery with a polymer-gel electrolyte and a polyaniline cathode. *Angewandte Chemie* 130:5547–5551. <https://doi.org/10.1002/anie.201802248>
33. Thanisha F, Koliyoor J, Ismayil MJ (2024) Amorphous magnesium-doped chitosan films as solid polymer electrolytes for energy storage device applications. *Mater Sci Eng, B* 301:117149. <https://doi.org/10.1016/j.mseb.2023.117149>
34. Kiruthika S, Malathi M, Selvasekarapandian S, Tamilarasan K, Maheshwari T (2020) Conducting biopolymer electrolyte based on pectin with magnesium chloride salt for magnesium battery application. *Polym Bull* 77:6299–6317. <https://doi.org/10.1007/s00289-019-03071-9>
35. Elia GA, Marquardt K, Hoepfner K, Fantini S, Lin R, Kinpping E, Peters W, Drillet JF, Passerini S, Hahn R (2016) An overview and future perspectives of aluminum batteries. *Adv Mater* 28:7564–7579. <https://doi.org/10.1002/adma.201601357>
36. Yang H, Li H, Li J, Sun Z, He K, Cheng HM, Li F (2019) The rechargeable aluminum battery: opportunities and challenges. *Angewandte Chemie* 35:11978–11996
37. Tiwari T, Pandey K, Srivastava N, Srivastava PC (2011) Effect of glutaraldehyde on electrical properties of arrowroot starch + NaI electrolyte system. *J Appl Polym Sci* 121:1–7. <https://doi.org/10.1002/app.33559>
38. D Yadav A, Pandey N, Srivastava 2024 Effect of crosslinker on the electrochemical properties of starch-based water-in-polymer-salt electrolytes <https://doi.org/10.1007/s11581-024-05689-w>
39. Yan L, Yang W, Yu H, Zhang L, Shu J (2023) Recent progress in rechargeable calcium-ion batteries for high-efficiency energy storage. *Energy Storage Mater* 60:102822
40. Shakourian-Fard M, Kamath G, Taimoory SM, Trant JF (2019) Calcium-ion batteries: identifying ideal electrolytes for next-generation energy storage using computational analysis. *J Phys Chem C* 123:15885–15896. <https://doi.org/10.1021/acs.jpcc.9b01655>
41. Ropp RC (2013) Group 17 (H, F, Cl, Br, I) Alkaline earth compounds. In: *Encyclopedia of the Alkaline Earth Compounds*. Elsevier, pp 25–104
42. Gao Y, Qin Z, Guan L, Wang X, Chen GZ (2015) Organoaqueous calcium chloride electrolytes for capacitive charge storage in carbon nanotubes at sub-zero-temperatures. *Chem Commun* 51:10819–10822. <https://doi.org/10.1039/c5cc03048j>
43. Zhang J, Cui C, Wang PF, Li Q, Chen L, Han F, Jin T, Liu S, Choudhary H, Raghavan SR, Eidson N (2020) “Water-in-salt” polymer electrolyte for Li-ion batteries. *Energy Environ Sci* 13:2878–2887. <https://doi.org/10.1039/d0ee01510e>
44. Samanta P, Ghosh S, Kolya H, Kang CW, Murmu NC, Kuila T (2021) Molecular crowded “water-in-salt” polymer gel electrolyte for an ultra-stable Zn-ion battery. *ACS Appl Mater Interfaces* 14:1138–1148
45. Khan Z, Ail U, Nadia Ajjan F, Phopase J, Ullah Khan Z, Kim N, Nilsson J, Inngan O, Berggren M, Crispin X (2022) Water-in-polymer salt electrolyte for slow self-discharge in organic batteries.

- Adv Energy Sustain Res 3:2100165. <https://doi.org/10.1002/aesr.202100165>
46. Suo L, Borodin O, Gao T, Olguin M, Ho J, Fan X, Luo C, Wang C (1979) Xu K (2015) “Water-in-salt” electrolyte enables high-voltage aqueous lithium-ion chemistries. *Science* 350:938–943. <https://doi.org/10.1126/science.aab1595>
47. Yadav M, Nautiyal G, Verma A, Kumar M, Tiwari T, Srivastava N (2019) Electrochemical characterization of NaClO₄–mixed rice starch as a cost-effective and environment-friendly electrolyte. *Ionics* 25:2693–2700. <https://doi.org/10.1007/s11581-018-2794-x>
48. Yadav M, Kumar M, Srivastava N (2018) Supercapacitive performance analysis of low cost and environment friendly potato starch based electrolyte system with anodized aluminium and Teflon coated carbon cloth as electrode. *Electrochim Acta* 283:1551–1559. <https://doi.org/10.1016/j.electacta.2018.07.060>
49. Yadav D, Basuroy S, Kumar R, Aggarwal K, Srivastava N (2024) Effect of high humidity exposure to wheat starch based high conducting flexible polymer-in-salt-electrolyte. *Macromol Symp* 413:2300068. <https://doi.org/10.1002/masy.202300068>
50. Tiwari T, Chauhan JK, Yadav M, Kumar M, Srivastava N (2017) Arrowroot + NaI: a low-cost, fast ion conducting eco-friendly polymer electrolyte system. *Ionics* 23:2809–2815. <https://doi.org/10.1007/s11581-017-2028-7>
51. Xiang C, Li M, Zhi M, Manivannan A, Wu N (2013) A reduced graphene oxide/Co₃O₄ composite for supercapacitor electrode. *J Power Sources* 226:65–70. <https://doi.org/10.1016/j.jpowsour.2012.10.064>
52. Wu Q, Xu Y, Yao Z, Liu A, Shi G (2010) Supercapacitors based on flexible graphene/polyaniline nanofiber composite films. *ACS Nano* 4:1963–1970. <https://doi.org/10.1021/nn1000035>
53. Ali A, Chiang YW, Santos RM (2022) X-ray diffraction techniques for mineral characterization: a review for engineers of the fundamentals, applications, and research directions. *Minerals* 12:205. <https://doi.org/10.3390/min12020205>
54. Xu W, Wang LM, Angell CA (2003) “PolyMOB”-lithium salt complexes: from salt-in-polymer to polymer-in-salt electrolytes. *Electrochim Acta* 48:2037–2045
55. St-Onge V, Cui M, Rochon S, Daigle JC, Claverie JP (2021) Reducing crystallinity in solid polymer electrolytes for lithium-metal batteries via statistical copolymerization. *Commun Mater* 2:83
56. Yadav M, Kumar M, Srivastava N (2023) High-conducting, economical, and flexible polymer-in-salt electrolytes (PISEs) suitable for energy devices: a reality due to glutaraldehyde crosslinked starch as host. *J Solid State Electrochem* 27:1213–1226. <https://doi.org/10.1007/s10008-023-05421-0>
57. Yadav M, Verma A, Nautiyal G, Srivastava N (2019) Magnesium perchlorate mixed and glutaraldehyde crosslinked potato starch: an economical and flexible electrolyte membrane. *Macromol Symp* 388:1900033. <https://doi.org/10.1002/masy.201900033>
58. Chauhan JK, Yadav D, Yadav M, Kumar M, Tiwari T, Srivastava N (2020) NaClO₄ added, corn and arrowroot starch based economical, high conducting electrolyte membranes for flexible energy devices. *SN Appl Sci* 2:1–12. <https://doi.org/10.1007/s42452-020-2660-0>
59. Pal B, Yang S, Ramesh S, Thangadurai V, Jose R (2019) Electrolyte selection for supercapacitive devices: a critical review. *Nanoscale Adv* 1:3807–3835. <https://doi.org/10.1039/c9na00374f>
60. Zhong C, Deng Y, Hu W, Qiao J, Zhang L, Zhang J (2015) A review of electrolyte materials and compositions for electrochemical supercapacitors. *Chem Soc Rev* 44:7484–7539
61. Oil O, Väärnõu M, Gorbatovski G, Zhao J, Siimenson C, Siinor L, Lusk K, Romann T, Pikma P, Lust E (2019) Adsorption of anions on bismuth and cadmium single crystal plane electrodes from various solvents and ionic liquid mixtures. *Electrochim Acta* 319:895–908. <https://doi.org/10.1016/j.electacta.2019.06.179>
62. Srivastava Neelam, Kumar Manindra, Tiwari Tuhina, Electrolysis of starch based electrolyte. 372370. 31–05–2012
63. Groves TS, Perez-Martinez CS, Lhermerout R, Perkin S (2021) Surface forces and structure in a water-in-salt electrolyte. *J Phys Chem Lett* 12:1702–1707. <https://doi.org/10.1021/acs.jpcclett.0c03718>
64. Shen Y, Liu B, Liu X, Liu J, Ding J, Zhong C, Hu W (2021) Water-in-salt electrolyte for safe and high-energy aqueous battery. *Energy Storage Mater* 34:461–474
65. Tot A, Zhang L, Berg EJ, Svensson PH, Kloo L (2023) Water-in-salt electrolytes made saltier by Gemini ionic liquids for highly efficient Li-ion batteries. *Sci Rep* 13:2154. <https://doi.org/10.1038/s41598-023-29387-1>
66. Avraham E, Yaniv B, Soffer A, Aurbach D (2008) Developing ion electroadsorption stereoselectivity, by pore size adjustment with chemical vapor deposition onto active carbon fiber electrodes. Case of Ca²⁺/Na⁺ Separation in water capacitive desalination. *J Phys Chem C* 112:7385–7389. <https://doi.org/10.1021/jp711706z>
67. Ranjithkumar R, Arasi SE, Sudhakar S, Nallamuthu N, Devendran P, Lakshmanan P, Kumar MK (2019) Enhanced electrochemical studies of ZnO/CNT nanocomposite for supercapacitor devices. *Physica B Condens Matter* 568:51–59. <https://doi.org/10.1016/j.physb.2019.05.025>
68. Chen YL, Hu ZA, Chang YQ, Wang HW, Zhang ZY, Yang YY, Wu HY (2011) Zinc oxide/reduced graphene oxide composites and electrochemical capacitance enhanced by homogeneous incorporation of reduced graphene oxide sheets in zinc oxide matrix. *J Phys Chem C* 115:2563–2571. <https://doi.org/10.1021/jp109597n>
69. Raghavendra KV, Vinoth R, Zeb K, Gopi CV, Sambasivam S, Kummara MR, Obaidat IM, Kim HJ (2020) An intuitive review of supercapacitors with recent progress and novel device applications. *J Energy Storage* 31:101652
70. Beyers I, Bensmann A, Hanke-Rauschenbach R (2023) Ragone plots revisited: a review of methodology and application across energy storage technologies. *J Energy Storage* 73:109097
71. Du H, Wu Z, Xu Y, Liu S, Yang H (2020) Poly(3,4-ethylenedioxythiophene) based solid-state polymer supercapacitor with ionic liquid gel polymer electrolyte. *Polymers* 12:297. <https://doi.org/10.3390/polym12020297>
72. Kötz R, Carlen MJ (2000) Principles and applications of electrochemical capacitors. *Electrochim Acta* 45:2483–2498. [https://doi.org/10.1016/S0013-4686\(00\)00354-6](https://doi.org/10.1016/S0013-4686(00)00354-6)
73. Figueroa-Gonzalez E, Mendoza R, Oliva AI, Gomez-Solis C, Valle-Garcia LS, Oliva E, Rodriguez-Gonzalez V, Encinas A, Oliva J (2021) Highly efficient and biodegradable flexible supercapacitors fabricated with electrodes of coconut-fiber/graphene nanoplates. *J Phys D Appl Phys* 55:035501. <https://doi.org/10.1088/1361-6463/ac2db5>
74. Hoseinizadeh M, Salem KE, Gouda A, Belanger D, Santato C (2023) Tannins for sustainable semi-solid-state supercapacitors. *Waste Biomass Valorization* 14:3475–88. <https://doi.org/10.1007/s12649-023-02125-4>
75. Feng C, Jia B, Wang H, Wang Y, Wu X (2023) A novel strategy for high energy density supercapacitors: formation of cyanuric acid between Ti3C2Tx (MXene) interlayer hybrid electrodes. *Chemical Eng J* 465:142935. <https://doi.org/10.1016/j.cej.2023.142935>

Publisher's Note Springer Nature remains neutral with regard to jurisdictional claims in published maps and institutional affiliations.

Springer Nature or its licensor (e.g. a society or other partner) holds exclusive rights to this article under a publishing agreement with the author(s) or other rightsholder(s); author self-archiving of the accepted manuscript version of this article is solely governed by the terms of such publishing agreement and applicable law.